Current–phase relation of a ballistic asymmetric double superconductor–normal-metal–superconductor junction

Victor C.Y. Chang, C.S. Chu*

Department of Electrophysics, National Chiao Tung University, Hsinchu 30050, Taiwan, ROC

Abstract

The zero-temperature current–phase (I–ϕ) relation (CPR) of a mesoscopic, ballistic, and asymmetrically stacked, double superconductor–normal-metal–superconductor (SNS) junction is studied. Here ϕ is the phase difference between the two superconducting end-electrodes. The lack of configuration symmetry in such asymmetric SNSNS junctions forbids a simple choice of values for the phase ϕ_2 of the middle superconductor. We propose to determine the values of ϕ_2 by equating the currents in the two normal regions. Two features in the CPR are found. First, the CPR of the asymmetric junction has a cutoff feature, whose origin is best demonstrated in the long middle superconductor (large L_2) cases, when the critical current of the double SNS junction is bounded by the SNS junction that has the longer normal region. This cutoff feature is more pronounced for longer L_2 and for higher degree of junction asymmetry. Second, in regions other than the cutoff region, the CPR of the asymmetric junction deviates only within a few percent from the CPR of the symmetric junction which has the same total length L_{Total} in the normal regions and the same L_2. This is in contrast with the greater sensitivity the CPR has to the changes in L_{Total} or L_2. © 1998 Elsevier Science B.V. All rights reserved.

1. Introduction

The possible manifestations of mesoscopic phenomena in transport properties of systems that have both normal and superconducting constituents have attracted much attention lately [1]. In these systems, the quasiparticles maintain their coherence in the normal regions while the Cooper pairs are, by nature, coherent in the superconducting regions [2]. The issue at hand is to look for the analogous manifestation in the physical characteristics of the superconducting systems for all mesoscopic phenomena found in normal systems.

This issue of analogy has prompted recent studies in double SNS (SNSNS) junctions, in which the effects of the resonant transmission of Cooper pairs [3], and the Andreev level tunneling [4] on the

* Corresponding author. Tel.: + 886-3-5720635; fax: + 886-3-5725230; e-mail: cschu@cc.nctu.edu.tw.

transport characteristics are considered. It was found that the dependence of the critical current on the distance between the two SNS junctions bears only a marginal resemblance to that of the resonant transmission [3]. On the other hand, we have shown recently that the current–phase relation (CPR) of a symmetric SNSNS junction, in the low temperature regime, bears unequivocal signatures of the Andreev level tunneling [4]. This result suggests that the CPR, rather than the critical current, is the more informative transport characteristics which we should turn to in looking for other analogous mesoscopic signatures. The CPR of a superconducting point contact has recently been observed by Koops et al. [5], and this has unveiled a very promising prospect for a direct probing of analogous mesoscopic signatures in the CPR, and in the near future.

In a mesoscopic superconducting junction, the pair-potential, together with its spatial profile, plays a more subtle role than the potential profile in normal systems. Besides that it gives rise to Andreev reflection at a SN interface, and that the reflection corresponds to the transmission of a Cooper pair, the pair-potential is, in general, complex and carries a phase ϕ. The role of this ϕ becomes even more interesting in structures that consist of other superconducting regions in between two superconducting end-electrodes. Examples of these structures, including SNSNS junctions [6,4] and superconducting superlattices [7], have recently been considered microscopically [8]. In these studies, ϕ is assumed constant within a superconducting region, and the structures are taken to have such symmetry that an intuitive choice for the phase difference $\Delta\phi$ between consecutive superconducting regions is possible. For a better understanding of the role of ϕ, we opt, in this paper, to remove the configuration symmetry, and consider an asymmetric SNSNS junction. The more complicated superconducting superlattice structures are left to further study.

As it turns out, the asymmetric SNSNS junction is more complicated than the symmetric junction. This is because the lack of symmetry in the junction forbids any simple choice of values for the phase ϕ_2 of the middle superconductor. To determine ϕ_2, we propose, in this paper, to adjust its value until

the supercurrent in the two normal regions are equal. The current expression is microscopically derived [9,4]. As we will show in this work, this method of determining ϕ_2 is consistent, in the large L_2 regime, with an intuitive approach which treats the double SNS junction as two independent but serially connected SNS junctions.

The paper is organized as follows. In Section 2, we briefly outline our approach for the calculation of the supercurrent in an asymmetric SNSNS junction. In Section 3, the analytic expressions for the quantization condition of the Andreev levels are derived. Numerical examples for the dependencies of ϕ_2, and the current on ϕ, in both the symmetric and the asymmetric junctions, are presented. Finally, we present a conclusion in Section 4.

2. Method

In this section, our method of calculation for the asymmetric SNSNS junctions is outlined, a detail account of the method can be found in our earlier paper [4].

The pair potential for an $S_1N_1S_2N_2S_3$ junction, as shown in Fig. 1, is given by

$$\Delta(x) = \begin{cases} \Delta_1 e^{i\phi_1}, & x < 0, \\ 0, & 0 < x < L_1, \\ \Delta_2 e^{i\phi_2}, & L_1 < x < L_1 + L_2, \\ 0, & L_1 + L_2 < x < L_1 + L_2 + L_3, \\ \Delta_1 e^{i\phi_3}, & x > L_1 + L_2 + L_3. \end{cases} \tag{1}$$

The energy gap magnitude Δ_1 of the two superconducting end-electrodes are taken to be the same. The energy gap of the middle superconductor can be different, and its phase ϕ_2 is determined by equating the supercurrents in the two normal regions. In this work, for simplicity, we have taken $\Delta_2 \leqslant \Delta_1$. The quasiparticles of the system are described by the Bogoliubov–de Gennes (BdG) equation

$$H(x)u(x) + \Delta(x)v(x) = Eu(x),$$
$$\Delta^*(x)u(x) - H^*(x)v(x) = Ev(x). \tag{2}$$

For quasiparticles with energies $E > \Delta_1$, they are scattering states resulting from either electron like
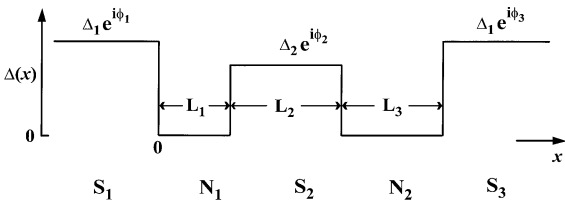
Fig. 1. Schematic representation of an $S_1N_1S_2N_2S_3$ junction with stepwise pair potentials.

or hole like quasiparticles incident from one of the superconducting end-electrodes. By invoking the Andreev approximation when matching the wave functions at the SN interfaces, we obtain the analytic expressions for the scattering states as well as their contribution to the supercurrent. The scattering coefficients are given in Appendix A.

For $E \leqslant \Delta_1$, the quasiparticles are confined in between the two end-electrodes and their energies are quantized. Furthermore, when $E < \Delta_2$, the quasiparticles are confined within, but can tunnel between, the two normal regions. We obtain the analytical expression for the quantization conditions for these bound states. There are two kinds of such bound states, according to the processes involved. The p process is set up by right-going electron like quasiparticles and the n process is set up by right-going hole like quasiparticles in the normal regions [10].

The supercurrent can be obtained using the current density expression

$$j(x) = \frac{e}{m} \sum_l \{ f(E_l) u_l^*(x) \hat{p}_x u_l(x)$$

$$+ [1 - f(E_l)] v_l(x) \hat{p}_x v_l^*(x) \} + \text{c.c.}, \quad (3)$$

where l refers to the quasiparticle states, continuous or discrete in the energy spectrum, with $E_l > 0$, and with the wave functions given by $[u_l(x), v_l(x)]^T$. Here $e = -|e|$, and $\hat{p}_x = -i\hbar \, d/dx - (e/c)A_x(x)$. The vector potential $A_x(x) = 0$ in our case. The function $f(\varepsilon) = [1 + \exp(\varepsilon/k_B T)]^{-1}$ is the Fermi function. In one dimension, the current density becomes the current.

The contribution of the discrete levels to the supercurrent is given by the sum over discrete levels in Eq. (3). There is, however, an alternate current

expression for the discrete levels, given by [9,6,8,11]

$$I_1 = -\frac{2e}{\hbar} \sum_l \tanh(E_l/2k_B T) \frac{dE_l}{d\phi}. \quad (4)$$

Here ϕ is the phase difference between the pair potentials of the two end-electrodes. For the contributions from the discrete levels, these two expressions are shown to be the same in SNS junctions and in symmetric SNSNS junctions [4].

Since Eq. (3) is local, containing the location at which the current is to be evaluated, we can calculate the currents in the two normal regions of the SNSNS junction. However, for a given phase difference ϕ across the entire junction, the currents depend also on the ϕ_2 of the middle superconductor. Hence ϕ_2 cannot be arbitrary. Rather, its values can be determined by equating the supercurrents in the two normal regions. In other words, ϕ_2 becomes a function of ϕ.

3. Results

In this section, we present the analytical expressions for the quantization conditions of the Andreev levels. We also present and interpret the numerical results for the CPR of SNSNS junctions, including both the long L_2 case, when the two SNS junctions can be considered as independent, and the short L_2 case, when Andreev tunneling effects are important.

3.1. Andreev levels

The quantization conditions for the Andreev levels can be simplified into a more compact form if the wave vectors $\tilde{k}_e = k_F\sqrt{1 + E/\mu}$, and $\tilde{k}_h = k_F\sqrt{1 - E/\mu}$, both in the normal regions, are kept up to the first order in E/μ, and the wave vectors in the superconducting region S_j,

$$k_{e,j} = k_F \sqrt{1 + \frac{\sqrt{E^2 - \Delta_j^2}}{\mu}},$$

and

$$k_{h,j} = k_F \sqrt{1 - \frac{\sqrt{E^2 - \Delta_j^2}}{\mu}}, \quad (5)$$

are kept up to the first order in $\sqrt{E^2 - \Delta_j^2}/\mu$. Here the subscripts e(h) refers to electronlike (holelike) quasiparticles, and $k_F = \sqrt{2m\mu}/\hbar$.

For the case $E \leqslant \Delta_2$, the quantization condition is

$$
\exp\left(\frac{\sqrt{\Delta_2^2 - E^2}k_F L_2}{2\mu}\right)\cos\left[\frac{Ek_F}{2\mu}(L_1 + L_3)\right.
$$
$$
\left. - \cos^{-1}\left(\frac{E}{\Delta_1}\right) - \cos^{-1}\left(\frac{E}{\Delta_2}\right) \mp \frac{\phi_{31}}{2}\right]
$$
$$
- \exp\left(-\frac{\sqrt{\Delta_2^2 - E^2}k_F L_2}{2\mu}\right)
$$
$$
\times \cos\left[\frac{Ek_F}{2\mu}(L_1 + L_3) - \cos^{-1}\left(\frac{E}{\Delta_1}\right)\right.
$$
$$
\left. + \cos^{-1}\left(\frac{E}{\Delta_2}\right) \mp \frac{\phi_{31}}{2}\right]
$$
$$
- \left[\exp\left(\frac{\sqrt{\Delta_2^2 - E^2}k_F L_2}{2\mu}\right)\right.
$$
$$
\left. - \exp\left(-\frac{\sqrt{\Delta_2^2 - E^2}k_F L_2}{2\mu}\right)\right]
$$
$$
\times \cos\left[\frac{Ek_F}{2\mu}(L_1 - L_3) \mp \left(\frac{\phi_{21}}{2} - \frac{\phi_{32}}{2}\right)\right] = 0, \quad (6)
$$

where the upper (lower) sign denotes the p process (n process), and $\phi_{ij} = \phi_i - \phi_j$. For convenience, we choose, in the following, that $\phi_1 = -\phi/2$, and $\phi_3 = \phi/2$. Hence the factor $(\phi_{21} - \phi_{32})/2 = \phi_2$ inside the cosine function in the last term of Eq. (6). In the case of a symmetric junction, when $L_1 = L_3$, $\phi_2 = 0$ is a reasonable choice so that ϕ appears as $\phi/2$ in the cosine functions of Eq. (6), and the Andreev levels $E(\phi)$ have a ϕ-period equal to 4π. But in an asymmetric junction, when $\phi_2 = \phi_2(\phi)$ through equating the supercurrents in the two normal regions, the dependence of Eq. (6) on ϕ becomes not at all obvious. It turns out, from our numerical results, and at $T = 0$, that the ϕ-period remains equal to 4π.

The exponential factors in Eq. (6) involve L_2, which represent the effects of the Andreev level tunneling. In the limit of infinite L_2, Eq. (6) becomes $Ek_F L_1/\mu - \arccos(E/\Delta_1) - \arccos(E/\Delta_2) \mp \phi_{21} = 2\pi n$, or $Ek_F L_3/\mu - \arccos(E/\Delta_1) -$ $\arccos(E/\Delta_2) \mp \phi_{32} = 2\pi n$, which are the quantization conditions for an asymmetric SNS junction with length L_1 or L_3, and with phase differences ϕ_{21} or ϕ_{32}, respectively [12]. In addition, at $E = 0$, the quantization condition becomes

$$
\cos\left(\frac{\phi}{2}\right) + \cos(\phi_2)\tanh\left(\frac{\Delta_2 k_F L_2}{2\mu}\right) = 0, \quad (7)
$$

from which the values of ϕ that satisfy $E(\phi) = 0$ are determined. The separation between these ϕ values changes with L_2, and is therefore a consequence of the Andreev level tunneling. In the vicinity of $E \approx 0$, an Andreev level changes from an n-process to a p-process, or vise versa, and the contribution of this level to the current is changed abruptly. It is also interesting to note that Eq. (7) does not depend explicitly on Δ_1, L_1, and L_3, but could depend on these junction parameters implicitly through ϕ_2. Our numerical results show that these ϕ_2 values are quite insensitive to L_1 or L_3 when their sum $L_{\text{Total}} = L_1 + L_3$ is fixed.

For the case when $\Delta_2 < E < \Delta_1$, the quantization condition becomes

$$
\frac{\sqrt{E^2 - \Delta_2^2}}{E}\cos\left(\frac{\sqrt{E^2 - \Delta_2^2}k_F L_2}{2\mu}\right)
$$
$$
\times \sin\left[\frac{Ek_F}{2\mu}(L_1 + L_3) - \cos^{-1}\left(\frac{E}{\Delta_1}\right) \mp \frac{\phi_{31}}{2}\right]
$$
$$
+ \sin\left(\frac{\sqrt{E^2 - \Delta_2^2}k_F L_2}{2\mu}\right)\cos\left[\frac{Ek_F}{2\mu}(L_1 + L_3)\right.
$$
$$
\left. - \cos^{-1}\left(\frac{E}{\Delta_1}\right) \mp \frac{\phi_{31}}{2}\right]
$$
$$
- \frac{\Delta_2}{E}\sin\left(\frac{\sqrt{E^2 - \Delta_2^2}k_F L_2}{2\mu}\right)
$$
$$
\times \cos\left[\frac{Ek_F}{2\mu}(L_1 - L_3) \mp \left(\frac{\phi_{21}}{2} - \frac{\phi_{32}}{2}\right)\right] = 0, \quad (8)
$$

where, again, the upper (lower) sign refers to the p process (n process). Taking $L_2 = 0$, the condition becomes that of a symmetric SNS junction with a normal region of length L_{Total} [13,14]. Taking another limit, $\Delta_2 = 0$, the condition becomes that of a symmetric SNS junction with a normal region of length $L_1 + L_2 + L_3$. There is no tunneling

feature in this case due to the obvious reason that $E > \Delta_2$. The quantization condition in the $E = \Delta_1$ limit is given in Appendix B. The expression for the supercurrent due to the scattering states is given in Appendix C.

3.2. Current-phase relations for SNSNS junctions with $L_2 \gg \xi$

We present, in this subsection, the results for SNSNS junctions that have a long middle superconductor. In this $L_2 \gg \xi$ regime, an intuitive picture arises. The coupling between the two SNS junctions via Andreev level tunneling becomes unimportant, and the SNSNS junctions can be regarded as two independent SNS junctions connected serially. Our numerical results conform with this intuitive picture.

In the following numerical examples, all the SNSNS junctions considered have the same $\Delta_1 = \Delta_2 = 0.2$ meV, $\mu = 10$ meV, and $T = 0$. The ratio $\Delta_1/\mu = 0.02$ is small enough such that the Andreev approximation is valid. These junctions are different, however, in L_1, L_3, the lengths of the two normal regions, and also in L_2. These lengths are expressed in units of $\xi = \mu/k_F\Delta_1$.

In Fig. 2, the CPRs of four SNSNS junctions are presented. For the symmetric junction where $(L_1, L_2, L_3) = (0.5, 10, 0.5)$, the CPR branch is represented by the bold curve. For the asymmetric junction $(0, 10, 1)$, the CPR is represented by the solid circles. The total length of the normal region $L_{\text{Total}} = 1$ is the same in both of the above junctions. The CPRs of the other two symmetric junctions, $(0, 10, 0)$ and $(1, 10, 1)$, are represented by the dashed and the thin solid curves. These CPRs all have a ϕ-period of 4π.
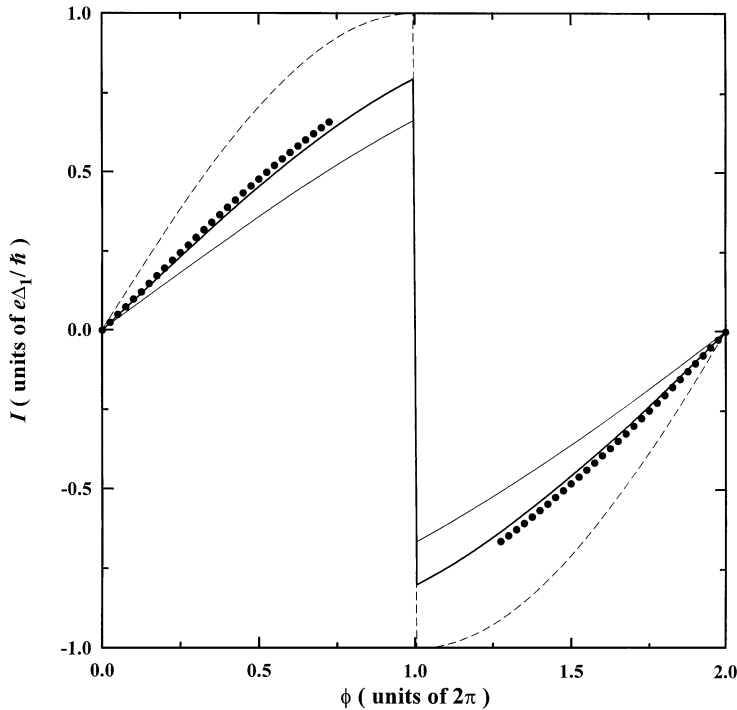

Fig. 2. Supercurrent versus ϕ for SNSNS junctions in which the length L_2 of the middle superconductor is long. For the purpose of comparison, we have plotted the CPR of four structures. The physical parameters that are the same among these structures are $\Delta_1 = \Delta_2 = 0.2$ meV, $\mu = 10$ meV, and $T = 0$. These structures differ by the lengths of the normal regions and the middle superconductor: (L_1, L_2, L_3), which are measured in units of ξ. The CPR for the structure $(L_1, L_2, L_3) = (0.5, 10, 0.5)$ is represented by the bold lines. The CPR for $(0, 10, 1)$, which has a cutoff feature, is represented by the solid circles. The other two structures $(0, 10, 0)$ and $(1, 10, 1)$ are represented by the dashed and the thin solid lines, respectively.

To present the physical meaning of the results in Fig. 2, we first focus on the symmetric SNSNS junctions, with $L_1 = 0, 0.5$, and 1, of which the CPRs are represented by the dashed, bold, and thin solid curves, respectively. Each of these CPRs has an abrupt current-change feature at $\phi = 2\pi$, and the critical current decreases as L_1 is increasing. Except for the ϕ-period, which is 4π, these CPRs resemble the CPRs of SNS junctions, whose ϕ-period is 2π. In fact, these $I(\phi)$ curves are found to be identical to $I_{\text{SNS}}(L_1, \phi/2)$, where $I_{\text{SNS}}(L_{\text{N}}, \phi)$ represents the supercurrent in an SNS junction that has a normal region of length L_{N} and a phase ϕ across the junction. This finding is consistent with the intuitive expectation that, for large L_2, the symmetric SNSNS junction becomes two identical SNS junctions connected in series.

The CPR of an SNS junction has been thoroughly studied theoretically in the recent past [9,13,14]. In the temperature regime $T \lesssim T_{\text{c}}$, the CPR is sinusoidal, as given by the Ginzburg–Landau results [15]. However in the temperature regime $T \ll T_{\text{c}}$, the CPR is nonsinusoidal and, at $T = 0$, has an abrupt current-change feature at $\phi = \pi$ [9,13,14]. The nonsinusoidal CPR feature has been confirmed by a recent experiment [5].

The $T = 0$ abrupt current change in the CPR is associated with a change in the process type of an Andreev level which has $E \approx 0$. According to Eq. (7), we see that there can be more than one abrupt current-change feature in the CPRs of SNSNS junctions, and the ϕ-separation between these features reflects directly the Andreev-level tunneling.

For the asymmetric SNSNS junction in Fig. 2, with $(L_1, L_2, L_3) = (0, 10, 1)$, it is found that the CPR deviates appreciably from that of the symmetric SNSNS junctions with $L_1 = 0, 1$, but deviates only within a few percent, whenever it has values, from that of the symmetric junction which has the same $L_{\text{Total}} = 1$. Besides, the CPR for the asymmetric junction has a cutoff feature in which the supercurrent is limited by that of the symmetric junction with $L_1 = 1$. This cutoff feature is consistent with the intuitive picture that, when L_2 is long enough, the SNSNS junction would behave like two independent SNS junctions connected in series. For an asymmetric SNSNS junction, the two SNS junc-

tions have different L_{N} and the critical current of the entire junction is determined by the SNS junction that has the longer L_{N}.

To show explicitly how this cutoff feature comes about in our calculation, we plot in Fig. 3 the

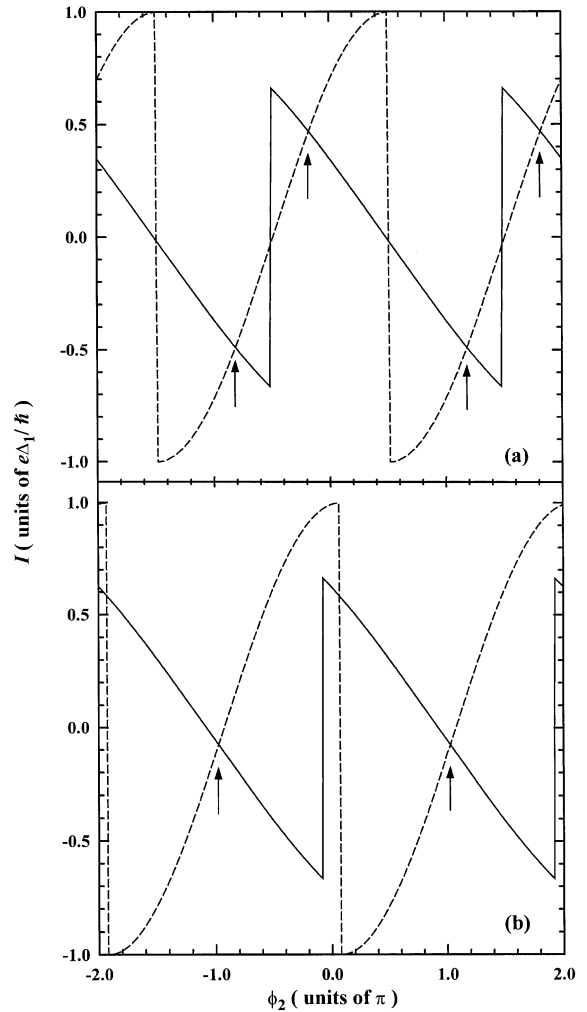Fig. 3. Supercurrent in the two normal regions versus ϕ_2. The SNSNS junction is the asymmetric junction in Fig. 2, in which L_2 is long and, in units of ξ, $(L_1, L_2, L_3) = (0, 10, 1)$. The phase difference across the entire junction is fixed at (a) $\phi/2\pi = 0.49$, and (b) $\phi/2\pi = 0.925$. The cutoff feature occurs in (b). The supercurrent evaluated in the normal region N_1 (N_2) is represented by the dashed (solid) curve, and is shown to resemble the CPR of a single SNS junction with the length L_{N} of the normal region equals 0 (1). The intersections between the two curves are indicated by arrows.

supercurrent versus ϕ_2 in the two normal regions, when ϕ is fixed. The asymmetric junction is the same as in Fig. 2. The $\phi/2\pi$ is 0.49 in Fig. 3a, and 0.925 in Fig. 3b. The supercurrent evaluated in the normal regions N_1, N_2 are represented by the dashed, and the solid curves, respectively, which are found to resemble the CPR of a single SNS junction. In fact, the current in the left SNS junction I_L equals $I_{SNS}(L_N = 0, \phi/2 + \phi_2)$, while the current in the right SNS junction I_R equals $I_{SNS}(L_N = 1, \phi/2 - \phi_2)$. Here $I_{SNS}(L_N, \phi)$ represents the super-current in an SNS junction that has a normal region of length L_N and a phase ϕ across the junction. This simply shows that the coupling between the two SNS junctions via Andreev level tunneling is unimportant for $L_2 = 10$. The intersections between these two curves, as indicated by arrows in Fig. 3, gives the possible values of I through the

asymmetric junction. The changes in the number of possible values for I, from two in Fig. 3a to one in Fig. 3b, indicate the occurrence of the cutoff feature. It is also clear that the critical current for the asymmetric junction should be limited by the critical current of I_R, the smaller critical current of the two SNS junctions. We note in passing that there is only one CPR branch, which has a ϕ-period of 4π, even though the two possible values of I in Fig. 3 seem to suggest a second CPR branch. The two CPR values, which are found to constitute the same CPR branch except for a relative shift $\Delta\phi$ of 2π, cannot be counted as two independent CPR branches, because the physical configuration of the junction is not changed by the transformation $\phi_i \rightarrow \phi_i + 2\pi n_i$ for integers n_i.

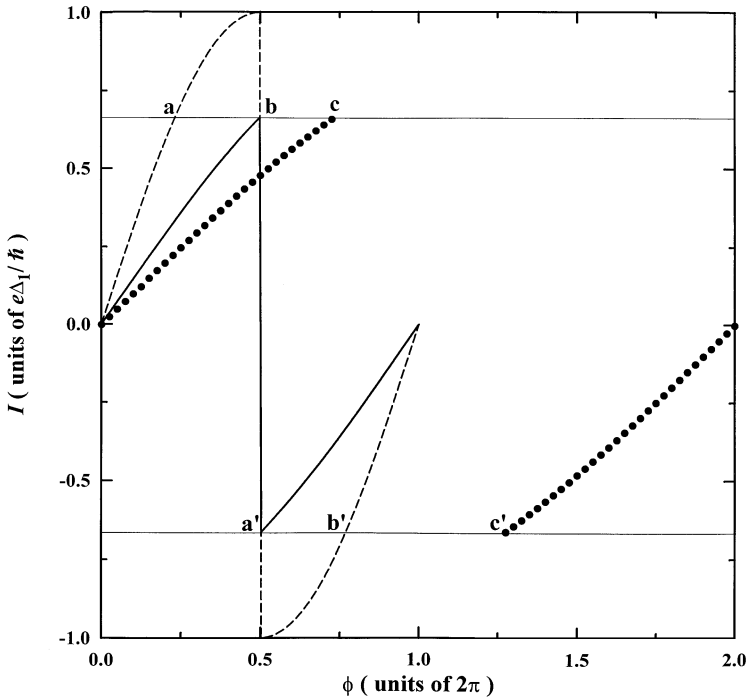In Fig. 4, we show that the CPR of the asymmetric junction can be constructed graphically from

Fig. 4. Constructing the CPR of an asymmetric and large L_2 SNSNS junction from the CPRs of the individual SNS junctions. The structure is the same as the asymmetric structure in Fig. 2. The CPR of the structure is represented by the solid circles. The CPRs of the single SNS junctions with $L_N = 0$, and 1 are represented by the dashed, and the solid curves, respectively. The two horizontal thin lines, which indicate the smallest critical current of the two SNS junctions, coincide with the cutoff feature in the CPR of the asymmetric junction. For a given supercurrent between the two horizontal thin lines, the corresponding phase ϕ for the CPR of the asymmetric junction can be obtained by adding the phases of the two individual SNS junctions. For example, $\phi_c = \phi_a + \phi_b$, and $\phi_{c'} = \phi_{a'} + \phi_{b'}$.

the CPRs of the two individual SNS junctions. The CPRs of the single SNS junctions, with $L_N = 0$, and 1, are, respectively, represented by the dashed and the solid curves. The CPR for the asymmetric junction is denoted by the solid circles. If the same current I is to flow through both of these SNS junctions, the total phase ϕ across the entire junction must be equal to the sum of the phases across the individual SNS junctions. As an example, in Fig. 4, we have $\phi_c = \phi_a + \phi_b$, and $\phi_{c'} = \phi_{a'} + \phi_{b'}$. The construction of the entire CPR branch for the asymmetric junction from the CPRs of the individual SNS follows quite straightforwardly. With this, we demonstrate that the large L_2 asymmetric junction is equivalent to two independent SNS junctions connected in series.

Our other results show that the deviation of the CPRs between an asymmetric and a symmetric junction, both having the same L_{Total}, increases

slowly with L_{Total}. In addition, the cutoff feature is more evident for larger L_{Total}. These can be understood according to the above construction scheme.

3.3. Current–phase relations for SNSNS junctions with intermediate L_2 values

In this subsection, the CPR for the asymmetric SNSNS junctions with shorter values of L_2, where the Andreev-level tunneling feature manifests, is presented. The numerical examples include junctions with short and intermediate L_{Total}.

The CPR for a junction with a short L_{Total} is presented in Fig. 5. The asymmetric junction has $(L_1, L_2, L_3) = (0.02, 1, 0.18)$, where $L_{\text{Total}} = 0.2$, and the CPR is denoted by the solid circles. For comparison, the CPR for a symmetric junction $(0.1, 1, 0.1)$, with the same L_{Total}, is presented. The
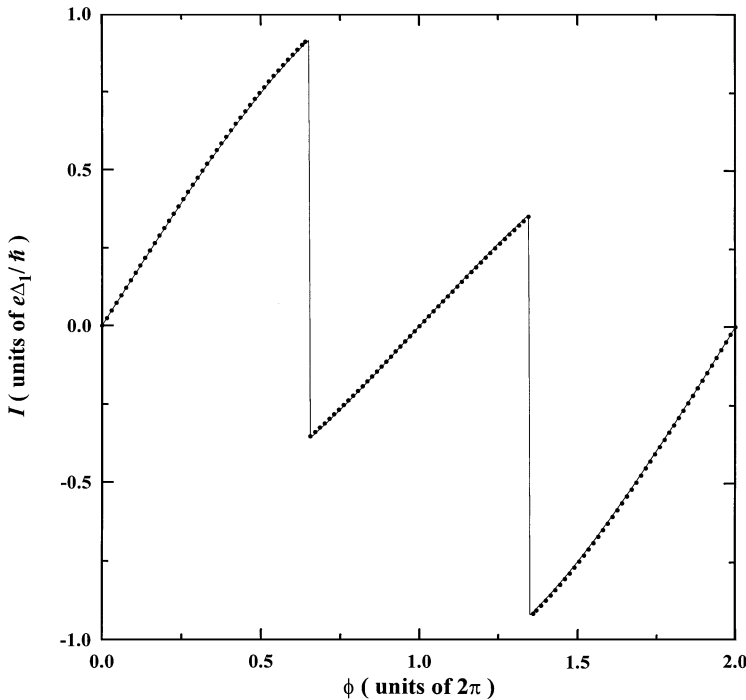

Fig. 5. Supercurrent versus ϕ for an asymmetric SNSNS junction with an intermediate L_2. The structure has $(L_1, L_2, L_3) = (0.02, 1, 0.18)$ and the CPR is represented by the solid circles. For comparison, we also present the CPR for the symmetric structure $(0.1, 1, 0.1)$ where the $L_{\text{Total}} = 0.2$ is the same in both structures. Other physical parameters are the same as in Fig. 2. Note that the CPRs for the two structures are essentially the same, and the cutoff feature in the CPR of the asymmetric junction is marginally shown by a missing solid circle each time when the CPR reaches the critical current value of the symmetric junction.

first feature to notice is that the CPRs for the two SNSNS junctions are essentially the same. Second, the cutoff feature is evident only under a scrutiny. The feature is marginally exhibited by a missing solid circle at each of the tips of the CPR near its critical current value. Third, there are two abrupt current-change features in a 4π ϕ-period, which are the manifestation of the coherent coupling between the two SNS junctions. In other words, the two SNS junctions are no longer independent.

The Andreev-level tunneling is the dominant factor governing the coherent coupling between the two SNS junctions. The connection between the Andreev-level tunneling and the occurrence of the two abrupt current-change features is understood for symmetric SNSNS junctions, which has been studied recently [4]. According to the discussions in the last subsection, the occurrence of the abrupt current-change feature simply reflects that an Andreev level switches from one process type to another, and the Andreev level must have energy very

close to zero. If the two SNS junctions of a symmetric SNSNS junction were independent, the Andreev levels in each SNS junction, including the $E \approx 0$ levels, would be degenerate for all ϕ values. But in the presence of the Andreev-level tunneling, the degeneracy in the Andreev levels is removed. Consequently there are two $E \approx 0$ Andreev levels, each occurring at a different ϕ, and each giving rise to an abrupt current-change feature in the CPR. Thus the CPR has two abrupt current-change features. This understanding holds essentially for the $E \approx 0$ Andreev levels in the asymmetric junctions.

In Fig. 6, the dependence of ϕ_2 on ϕ for the CPR of the asymmetric junction in Fig. 5 is plotted, and is denoted by the solid curves. The curves are piecewise linear and have values in the vicinity of $\phi_2 = n\pi$, which are the values of ϕ_2 for a symmetric junction. There are abrupt changes in ϕ_2, for the asymmetric junction, at $\phi/2\pi = 0.35, 0.65, 1.35,$ and 1.65. These ϕ values are the same as where the abrupt current-change features occur in Fig. 5.
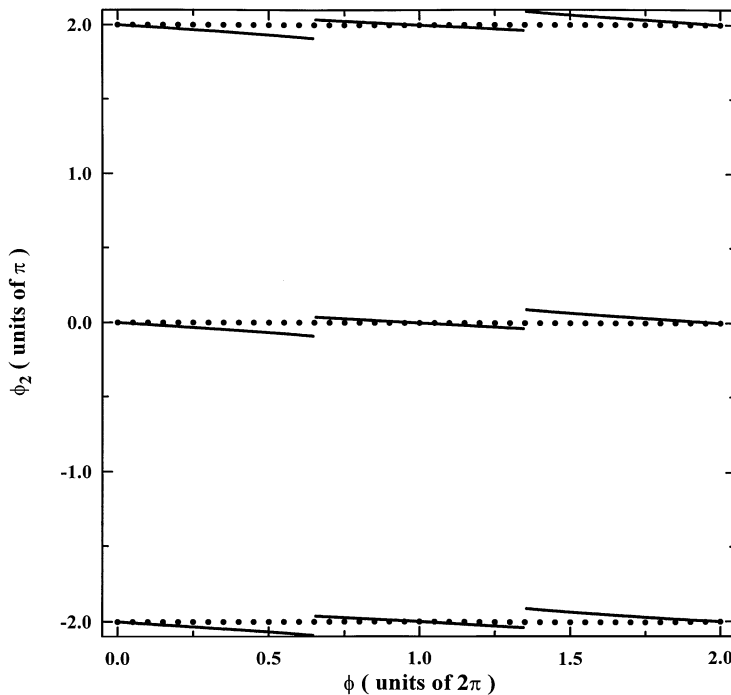

Fig. 6. ϕ_2 versus ϕ for an asymmetric SNSNS junction. The asymmetric structure is the same as in Fig. 5, and $\phi_2(\phi)$ is represented by the solid curves. There are abrupt changes in ϕ_2 at $\phi/2\pi = 0.35, 0.65, 1.35,$ and 1.65. For comparison, the $\phi_2(\phi)$ for a symmetric structure is represented by the solid circles. Note that $\phi_2 = n\pi$ for the symmetric structure.
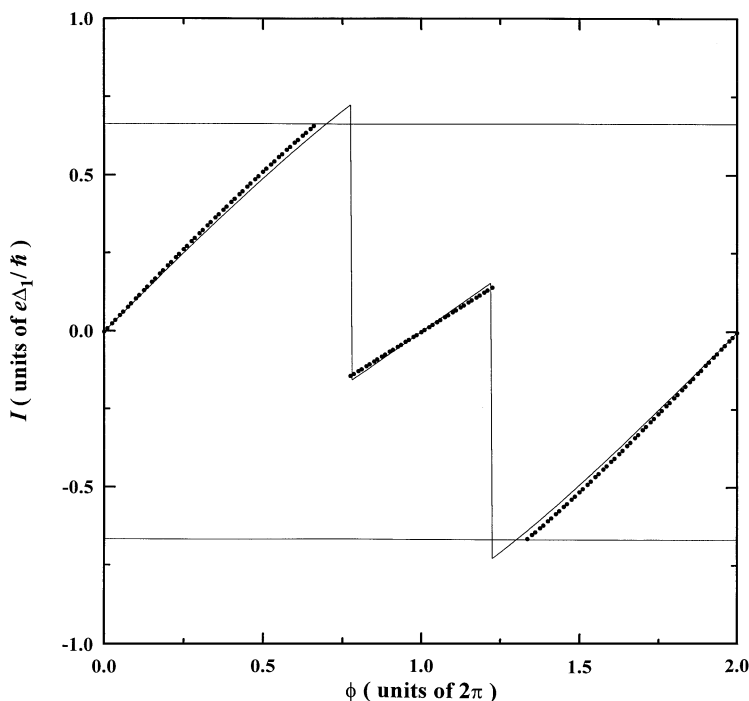
Fig. 7. Supercurrent versus ϕ for an asymmetric SNSNS junction with an intermediate L_{Total}. The structure has $(L_1, L_2, L_3) = (0, 2, 1)$, and the other physical parameters are the same as in Fig. 2. The CPR is represented by the solid circles. For comparison, the CPR for the symmetric junction with structure $(0.5, 2, 0.5)$ is represented by the solid curves. The two horizontal thin lines indicate the cutoff feature of the CPR in the asymmetric junction.

Finally, the CPR for a junction with intermediate L_{Total} and L_2 is presented in Fig. 7. The asymmetric junction has $(L_1, L_2, L_3) = (0, 2, 1)$, where $L_{Total} = 1$, and the CPR is denoted by the solid circles. For comparison, the CPR for a symmetric junction $(0.5, 2, 0.5)$, with the same L_{Total}, is presented. The cutoff feature is more evident than the junctions with smaller L_{Total}. There are two abrupt-current-change features, showing the effect of the Andreev level tunneling. The deviation between the CPR for the asymmetric and the symmetric junctions is larger than the corresponding deviation in Fig. 5. These results indicate that the deviation and the cutoff features are more pronounced for longer L_2 and for configurations with higher degree of asymmetry.

4. Conclusion

In conclusion, we have studied the supercurrent characteristics in an asymmetric SNSNS junction.

Our result shows that the current–phase relation has a cutoff feature, and that in regions other than the cutoff region, the CPR becomes insensitive to the position of the middle superconductor if the total length of the normal regions remains a constant.

Acknowledgements

Appendix A. Transmission coefficients

For an electron like quasiparticle incident from the left-hand side of the junction, the $t_{e(h)}$, and the $r_{e(h)}$ coefficients of the wave function are obtained,

given by

$$r_e = 0, \quad r_h = \frac{\mathcal{G}(E, \phi_{32}, \phi_{21})}{\mathcal{D}(E, \phi_{21}, \phi_{32})},$$

$$t_h = 0, \quad t_e = \frac{\mathcal{K}(E, \phi_{32})}{\mathcal{D}(E, \phi_{21}, \phi_{32})}, \tag{A1}$$

where

$$\begin{aligned}
\mathcal{G}(E, \theta_1, \theta_2) &= \exp[i(\tilde{k}_e L_1 + k_{e,2} L_2 + \tilde{k}_e L_3 - \theta_1)] \\
&\quad \times u_1 v_1 u_2^2 - \exp[i(\tilde{k}_h L_1 + k_{h,2} L_2 \\
&\quad + \tilde{k}_h L_3 + \theta_2)] u_1 v_1 u_2^2 \\
&\quad - \exp[i(\tilde{k}_e L_1 + k_{e,2} L_2 + \tilde{k}_h L_3)] u_1^2 u_2 v_2 \\
&\quad + \exp[i(\tilde{k}_e L_1 + k_{h,2} L_2 + \tilde{k}_h L_3)] u_1^2 u_2 v_2 \\
&\quad - \exp[i(\tilde{k}_h L_1 + k_{e,2} L_2 + \tilde{k}_e L_3 \\
&\quad - \theta_1 + \theta_2)] v_1^2 u_2 v_2 + \exp[i(\tilde{k}_h L_1 + k_{h,2} L_2 \\
&\quad + \tilde{k}_e L_3 - \theta_1 + \theta_2)] v_1^2 u_2 v_2 \\
&\quad + \exp[i(\tilde{k}_h L_1 + k_{e,2} L_2 \\
&\quad + \tilde{k}_h L_3 + \theta_2)] u_1 v_1 v_2^2 \\
&\quad - \exp[i(\tilde{k}_e L_1 + k_{h,2} L_2 \\
&\quad + \tilde{k}_e L_3 - \theta_1)] u_1 v_1 v_2^2, \tag{A2}
\end{aligned}$$

and

$$\begin{aligned}
\mathcal{K}(E, \theta) &= \exp\{i[(\tilde{k}_h + \tilde{k}_e - k_{e,1})(L_1 + L_3) \\
&\quad + (k_{h,2} + k_{e,2} - k_{e,1}) L_2 - \theta]\} \\
&\quad \times (u_1^2 - v_1^2)(u_2^2 - v_2^2). \tag{A3}
\end{aligned}$$

The transmission and the reflection coefficients are defined in terms of the $t_{e(h)}$ and the $r_{e(h)}$ coefficients, given by

$$T_{L \to R}^e(E, \phi, \phi_2) = |t_e|^2, \tag{A4}$$

$$R_{L \to R}^h(E, \phi, \phi_2) = |r_h|^2. \tag{A5}$$

We have checked that $T_{L \to R}^e + R_{L \to R}^h = 1$, which is expected because the BdG equation is Hermitian.

For a holelike quasiparticle incident from the left hand side of the junction, the $t_{e(h)}$ and the $r_{e(h)}$ coef-

ficients are

$$r_h = 0, \quad r_e = \frac{\mathcal{G}'(E, -\phi_{21}, -\phi_{32})}{\mathcal{D}'(E, -\phi_{32}, -\phi_{21})},$$

$$t_e = 0, \quad t_h = \frac{\mathcal{K}'(E, -\phi_{32})}{\mathcal{D}'(E, -\phi_{32}, -\phi_{21})}, \tag{A6}$$

where

$$\begin{aligned}
\mathcal{G}'(E, \theta_1, \theta_2) &= \exp[i(\tilde{k}_e L_1 + k_{e,2} L_2 + \tilde{k}_e L_3 - \theta_1)] \\
&\quad \times u_1 v_1 u_2^2 - \exp[i(\tilde{k}_h L_1 + k_{h,2} L_2 \\
&\quad + \tilde{k}_h L_3 + \theta_2)] u_1 v_1 u_2^2 \\
&\quad - \exp[i(\tilde{k}_e L_1 + k_{e,2} L_2 + \tilde{k}_h L_3 \\
&\quad - \theta_1 + \theta_2)] u_1^2 u_2 v_2 \\
&\quad + \exp[i(\tilde{k}_e L_1 + k_{h,2} L_2 + \tilde{k}_h L_3 \\
&\quad - \theta_1 + \theta_2)] u_1^2 u_2 v_2 \\
&\quad - \exp[i(\tilde{k}_h L_1 + k_{e,2} L_2 + \tilde{k}_e L_3)] v_1^2 u_2 v_2 \\
&\quad + \exp[i(\tilde{k}_h L_1 + k_{h,2} L_2 + \tilde{k}_e L_3)] v_1^2 u_2 v_2 \\
&\quad + \exp[i(\tilde{k}_h L_1 + k_{e,2} L_2 + \tilde{k}_h L_3 \\
&\quad + \theta_2)] u_1 v_1 v_2^2 - \exp[i(\tilde{k}_e L_1 + k_{h,2} L_2 \\
&\quad + \tilde{k}_e L_3 - \theta_1)] u_1 v_1 v_2^2, \tag{A7}
\end{aligned}$$

and

$$\begin{aligned}
\mathcal{K}'(E, \theta) &= \exp\{i[k_{h,1}(L_1 + L_2 + L_3) + \theta]\} \\
&\quad \times (u_1^2 - v_1^2)(u_2^2 - v_2^2). \tag{A8}
\end{aligned}$$

Again, the transmission and the reflection coefficients are defined as

$$T_{L \to R}^h(E, \phi, \phi_2) = |t_h|^2, \tag{A9}$$

$$R_{L \to R}^e(E, \phi, \phi_2) = |r_e|^2, \tag{A10}$$

where we have checked that $T_{L \to R}^h + R_{L \to R}^e = 1$.

For an electron like quasiparticle incident from the right-hand side of the junction, the $t_{e(h)}$ and the $r_{e(h)}$ coefficients are

$$r_e = 0, \quad r_h = \frac{\mathcal{G}''(E, -\phi_{21}, -\phi_{32})}{\mathcal{D}'(E, -\phi_{32}, -\phi_{21})},$$

$$t_h = 0, \quad t_e = \frac{\mathcal{K}(E, -\phi_{21})}{\mathcal{D}'(E, -\phi_{32}, -\phi_{21})}, \tag{A11}$$

where $\mathscr{G}''$ is the same as $\mathscr{G}$ except that L_1 and L_3 are interchanged.

For a hole like quasiparticle incident from the right hand side of the junction, the $t_{e(h)}$ and the $r_{e(h)}$ coefficients are

$$r_h = 0, \quad r_e = \frac{\mathscr{G}'''(E,\phi_{32},\phi_{21})}{\mathscr{D}(E,\phi_{21},\phi_{32})},$$

$$t_e = 0, \quad t_h = \frac{\mathscr{K}'(E,\phi_{21})}{\mathscr{D}(E,\phi_{21},\phi_{32})}, \tag{A12}$$

where $\mathscr{G}'''$ is the same as $\mathscr{G}'$ except that L_1 and L_3 are interchanged.

We note that our results are for general normal-region lengths L_1 and L_3. And our transmission coefficients reduce to that obtained by Hurd and Wendin [6] when taking the $L_1 = L_3 = 0$ limit.

Appendix B. Quantization condition ($E = \Delta_1$)

Both the bound state supercurrent I_d and the scattering state supercurrent I_s have kink features which occur at the ϕ's when new Andreev levels appear at $E = \Delta_1$. The conditions for finding these ϕ's are given by

$$\frac{\phi}{2} + 2n\pi = \pm \left[\frac{\Delta_1 k_F}{2\mu}(L_1 + L_3) + \tan^{-1}\beta \right.$$
$$\left. - \sin^{-1}\gamma \right]$$

$$\frac{\phi}{2} + 2n\pi = \pm \left[\frac{\Delta_1 k_F}{2\mu}(L_1 + L_3) + \tan^{-1}\beta \right.$$
$$\left. + \sin^{-1}\gamma - \pi \right], \tag{B1}$$

where n in an arbitrary integer, and the upper (lower) signs represent the conditions for the p process (n process). Here,

$$\beta = \tan\left(\frac{\sqrt{\Delta_1^2 - \Delta_2^2}k_F L_2}{2\mu} \right) \Big/ \sqrt{1 - (\Delta_2/\Delta_1)^2}, \tag{B2}$$

and

$$\gamma = \frac{\left(\dfrac{\Delta_2}{\Delta_1}\right)\sin\left(\dfrac{\sqrt{\Delta_1^2 - \Delta_2^2}k_F L_2}{2\mu}\right)\cos\left[\dfrac{\Delta_1 k_F}{2\mu}(L_1 - L_3)\right]}{\sqrt{1 - \left[\left(\dfrac{\Delta_2}{\Delta_1}\right)\cos\left(\dfrac{\sqrt{\Delta_1^2 - \Delta_2^2}k_F L_2}{2\mu}\right)\right]^2}}. \tag{B3}$$

Appendix C. Supercurrent

The supercurrent given by Eq. (3) includes contribution from both the Andreev levels and the scattering states. Our results show that the total supercurrent in the two normal regions are not the same for arbitrary values of ϕ_2. And when ϕ_2 is chosen such that the total supercurrent becomes the same in the two normal regions, it is found that the contribution from the Andreev levels, or, separately, that from the scattering states, do not necessarily equal in the two normal regions.

The supercurrent I_{s1} due to the scattering states, and evaluated in the normal region N_1, is given by

$$I_{s1} = -\frac{2e}{h}\int_{\Delta_1}^{\sqrt{\mu^2 + \Delta_1^2}} dE \frac{E}{\sqrt{E^2 - \Delta_1^2}}\tanh(E/2k_B T)$$

$$\times \left[\frac{\mathscr{F}_1(E,\phi_{32})}{|\mathscr{D}(E,\phi_{21},\phi_{32})|^2} - \frac{\mathscr{F}_1(E,-\phi_{32})}{|\mathscr{D}'(E,-\phi_{32},-\phi_{21})|^2} \right]$$

$$\times (u_1^2 - v_1^2)^2, \tag{C1}$$

where

$$\mathscr{D}(E,\theta_1,\theta_2) = \exp[i(\tilde{k}_h L_1 + k_{h,2}L_2 + \tilde{k}_h L_3 + \theta_1)]u_1^2 u_2^2$$
$$- \exp[i(\tilde{k}_e L_1 + k_{e,2}L_2 + \tilde{k}_e L_3 - \theta_2)]u_2^2 v_1^2$$
$$+ \{\exp[i(\tilde{k}_e L_1 + k_{e,2}L_2 + \tilde{k}_h L_3)]$$
$$+ \exp[i(\tilde{k}_h L_1 + k_{e,2}L_2 + \tilde{k}_e L_3 + \theta_1 - \theta_2)]$$
$$- \exp[i(\tilde{k}_h L_1 + k_{h,2}L_2 + \tilde{k}_e L_3 + \theta_1 - \theta_2)]$$
$$- \exp[i(\tilde{k}_e L_1 + k_{h,2}L_2 + \tilde{k}_h L_3)]\}u_1 u_2 v_1 v_2$$
$$- \exp[i(\tilde{k}_h L_1 + k_{e,2}L_2 + \tilde{k}_h L_3 + \theta_1)]u_1^2 v_2^2$$
$$+ \exp[i(\tilde{k}_e L_1 + k_{h,2}L_2 + \tilde{k}_e L_3 - \theta_2)]v_1^2 v_2^2, \tag{C2}$$

$$
\begin{aligned}
\mathscr{D}'(E, \theta_1, \theta_2) =\ & \exp[\mathrm{i}(\tilde{k}_{\mathrm{h}}L_1 + k_{\mathrm{h},2}L_2 + \tilde{k}_{\mathrm{h}}L_3 + \theta_1)]u_1^2 u_2^2 \\
& - \exp[\mathrm{i}(\tilde{k}_{\mathrm{e}}L_1 + k_{\mathrm{e},2}L_2 + \tilde{k}_{\mathrm{e}}L_3 - \theta_2)]u_2^2 v_1^2 \\
& + \{\exp[\mathrm{i}(\tilde{k}_{\mathrm{e}}L_1 + k_{\mathrm{e},2}L_2 + \tilde{k}_{\mathrm{e}}L_3)] \\
& + \exp[\mathrm{i}(\tilde{k}_{\mathrm{e}}L_1 + k_{\mathrm{e},2}L_2 + \tilde{k}_{\mathrm{h}}L_3 + \theta_1 - \theta_2)] \\
& - \exp[\mathrm{i}(\tilde{k}_{\mathrm{e}}L_1 + k_{\mathrm{h},2}L_2 + \tilde{k}_{\mathrm{h}}L_3 + \theta_1 - \theta_2)] \\
& - \exp[\mathrm{i}(\tilde{k}_{\mathrm{h}}L_1 + k_{\mathrm{h},2}L_2 + \tilde{k}_{\mathrm{e}}L_3)]\}u_1 u_2 v_1 v_2 \\
& - \exp[\mathrm{i}(\tilde{k}_{\mathrm{h}}L_1 + k_{\mathrm{e},2}L_2 + \tilde{k}_{\mathrm{h}}L_3 + \theta_1)]u_1^2 v_2^2 \\
& + \exp[\mathrm{i}(\tilde{k}_{\mathrm{e}}L_1 + k_{\mathrm{h},2}L_2 + \tilde{k}_{\mathrm{e}}L_3 - \theta_2)]v_1^2 v_2^2,
\end{aligned} \tag{C3}
$$

and

$$
\begin{aligned}
\mathscr{F}_1(E, \theta) =\ & u_2^4 + v_2^4 - 2[\,-\cos(\theta + \tilde{k}_{\mathrm{h}}L_3 \\
& - \tilde{k}_{\mathrm{e}}L_3 - k_{\mathrm{e},2}L_2 + k_{\mathrm{h},2}L_2)u_1 v_1 u_2^3 v_2 \\
& + \cos(\theta + \tilde{k}_{\mathrm{h}}L_3 - \tilde{k}_{\mathrm{e}}L_3)u_1 v_1 u_2^3 v_2 \\
& + \cos(k_{\mathrm{h},2}L_2 - k_{\mathrm{e},2}L_2)u_1^2 u_2^2 v_2^2 \\
& + \cos(k_{\mathrm{e},2}L_2 - k_{\mathrm{h},2}L_2)v_1^2 u_2^2 v_2^2 \\
& + \cos(\theta + \tilde{k}_{\mathrm{h}}L_3 - \tilde{k}_{\mathrm{e}}L_3)u_1 v_1 u_2 v_2^3 \\
& - \cos(\theta + \tilde{k}_{\mathrm{h}}L_3 - \tilde{k}_{\mathrm{e}}L_3 + k_{\mathrm{e},2}L_2 - k_{\mathrm{h},2}L_2) \\
& \times u_1 v_1 u_2 v_2^3\,].
\end{aligned} \tag{C4}
$$

Here

$$
u_j^2 = \frac{1}{2}\left(1 + \frac{\sqrt{E^2 - \Delta_j^2}}{E}\right),
$$

$$
v_j^2 = \frac{1}{2}\left(1 - \frac{\sqrt{E^2 - \Delta_j^2}}{E}\right). \tag{C5}
$$

The supercurrent $I_{\mathrm{s}2}$ due to the scattering states, and evaluated in the N_2 region, is the same as

$I_{\mathrm{s}1}$ except that the arguments $\pm\phi_{32}$ of $\mathscr{F}_1$ in Eq. (C1) is substitued by $\pm\phi_{21}$, and L_3 in Eq. (C4) is replaced by L_1.

We also have obtained the expressions for the supercurrent due to the bound states in the two normal regions. But we choose to present their numerical results in this paper instead of their expressions, because of the length of these expressions.

References

[1] See the review by T.M. Klapwijk, Physica B 197 (1994) 481, and the conference papers in 203 (1994) 201.
[2] I.O. Kulik, A.N. Omel'yanchuk, Fiz. Nisk. Temp. 3 (1977) 945; 4 (1978) 296 [Sov. J. Low Temp. Phys. 3 (1977) 459; 4 (1978) 142].
[3] F. Sols, J. Ferrer, I. Zapata, Physica B 203 (1994) 467; I. Zapata, F. Sols, Phys. Rev. B 53 (1996) 6693.
[4] V.C.Y. Chang, C.S. Chu, Phys. Rev. B 55 (1997) 6004.
[5] M.C. Koops, G.V. van Duyneveldt, R.de B. Ouboter, Phys. Rev. Lett. 77 (1996) 2542.
[6] M. Hurd, G. Wendin, Phys. Rev. B 51 (1995) 3754.
[7] Y. Tanaka, M. Tsukada, Phys. Rev. B 44 (1991) 7578.
[8] C.W.J. Beenakker, H. van Houten, in: W.P. Kirk, M.A. Reed (Eds.), Nanostructures and Mesoscopic Systems, Academic Press, New York, 1992, p. 481.
[9] C.W.J. Beenakker, H. van Houten, Phys. Rev. Lett. 66 (1991) 3056.
[10] S. Kashiwaya, Y. Tanaka, M. Koyanagi, K. Kajimura, Jpn. J. Appl. Phys. 34 (1995) 4555.
[11] P.W. Anderson, in: E.R. Caianiello (Ed.), The Many-body Problem, vol. 2, Academic Press, New York, 1964, p. 113.
[12] L. Chang, P.F. Bagwell, Phys. Rev. B 49 (1994) 15853.
[13] I.O. Kulik, Zh. Eksp. Teor. Fiz. 57 (1969) 1745 [Sov. Phys. JETP 30 (1970) 944].
[14] P.F. Bagwell, Phys. Rev. B 46 (1992) 12573.
[15] L.G. Aslamazov, A.I. Larkin, Zh. Eksp. Teor. Fiz. 9 (1969) 15 [Sov. Phys. JETP 9 (1969) 87].